Nonlinear Ptychographic Coherent Diffractive Imaging

M. Odstrcil,[1,2,*] P. Baksh,[1] C. Gawith,[1,3] R. Vrcelj,[4] J. G. Frey,[5] and W. S. Brocklesby[1]

[1]*Optoelectronics Research Centre, University of Southampton, SO17 1BJ, UK*
[2]*RWTH Aachen University, Experimental Physics of EUV, JARA-FIT, Steinbachstrasse 15, 52074 Aachen, Germany*
[3]*Covesion, Ltd., Romsey SO51 9DG, UK*
[4]*Centre for Defence Chemistry, Cranfield University, Shrivenham, SN6 8LA, UK*
[5]*Chemistry, Faculty of Natural and Environmental Sciences, University of Southampton, Southampton, SO17 1BJ, UK*

*mo1e13@soton.ac.uk

Abstract: Ptychographic Coherent Diffractive Imaging (PCDI) is a significant advance in imaging allowing the measurement of the full electric field at a sample without use of any imaging optics. So far it has been confined solely to imaging of linear optical responses. In this paper we show that because of the coherence-preserving nature of nonlinear optical interactions, PCDI can be generalised to nonlinear optical imaging. We demonstrate second harmonic generation PCDI, directly revealing phase information about the nonlinear coefficients, and showing the general applicability of PCDI to nonlinear interactions.

OCIS codes: 110.0110 Imaging systems; 110.1650 Coherence imaging, 180.4315 Nonlinear microscopy

References and links

1. R. Carriles, D. N. Schafer, K. E. Sheetz, J. J. Field, R. Cisek, V. Barzda, A. W. Sylvester, and J. A. Squier, "Invited Review Article: Imaging techniques for harmonic and multiphoton absorption fluorescence microscopy," Review of Scientific Instruments **80**, 081101 (2009).
2. M. D. Seaberg, B. Zhang, D. F. Gardner, E. R. Shanblatt, M. M. Murnane, H. C. Kapteyn, and D. E. Adams, "Tabletop nanometer extreme ultraviolet imaging in an extended reflection mode using coherent Fresnel ptychography," Optica **1**, 39 (2014).
3. G. Zheng, R. Horstmeyer, and C. Yang, "Wide-field, high-resolution Fourier ptychographic microscopy," Nature Photonics **7**, 739–745 (2013).
4. B. Abbey, K. A. Nugent, G. J. Williams, J. N. Clark, A. G. Peele, M. A. Pfeifer, M. de Jonge, and I. McNulty, "Keyhole coherent diffractive imaging," Nature Physics **4**, 394–398 (2008).
5. J. Miao, P. Charalambous, J. Kirz, and D. Sayre, "Extending the methodology of x-ray crystallography to allow imaging of micrometre-sized non-crystalline specimens," Nature **400**, 342–344 (1999).
6. J. Miao, T. Ishikawa, I. K. Robinson, and M. M. Murnane, "Beyond crystallography: Diffractive imaging using coherent x-ray light sources," Science **348**, 530–535 (2015).
7. K. A. Nugent, "Coherent methods in the X-ray sciences," Advances in Physics **59**, 1–99 (2010).
8. A. Yariv, "Quantum Electronics," p. 704 (1989).

9. M. Guizar-Sicairos, M. Holler, A. Diaz, J. Vila-Comamala, O. Bunk, and A. Menzel, "Role of the illumination spatial-frequency spectrum for ptychography," Physical review B **86**, 100103 (2012).
10. A. M. Maiden and J. M. Rodenburg, "An improved ptychographical phase retrieval algorithm for diffractive imaging," Ultramicroscopy **109**, 1256–1262 (2009).
11. M. Houe and P. D. Townsend, "An introduction to methods of periodic poling for second-harmonic generation," Journal of Physics D: Applied Physics **28**, 1747–1763 (1995).
12. O. Gayer, Z. Sacks, E. Galun, and A. Arie, "Temperature and wavelength dependent refractive index equations for MgO-doped congruent and stoichiometric LiNbO3," Applied Physics B **91**, 343–348 (2008).
13. R. T. Bailey, G. Bourhill, F. R. Cruickshank, D. Pugh, J. N. Sherwood, and G. S. Simpson, "Linear and nonlinear optical properties of the organic nonlinear material 4-nitro-4'-methylbenzylidene aniline," Journal of Applied Physics **73**, 1591–1597 (1993).

1. Introduction

Nonlinear optical processes have been the source of many novel and useful imaging modalities over the last 30 years. Information gained using nonlinear techniques extends that obtained through conventional linear optical microscopy, for example Coherent Anti-Stokes Raman (CARS) microscopy allows bond-specific imaging via the Raman effect to enable identification of chemical compounds without fluorescent tagging. Nonlinear optical microscopy is generally performed by scanning a suitable laser across a sample, and collecting the generated signal point-by-point [1].

The area of linear imaging is undergoing a transformation because of the development of a range of new coherent imaging techniques, collectively known as ptychographic coherent diffractive imaging (PCDI); in these techniques, the use of an objective lens is made unnecessary by the use of algorithmic recovery of the phase information lost when the intensity of scattered light incident on a detector is measured. The lost phase information is recovered using extra information as constraints. This technique originated from X-ray diffraction, but is now used in many wavelength regimes. PCDI provides many advantages over traditional transmission microscopy such as greater flexibility of the imaging setup [2–4], and imaging in the X-ray region of the spectrum is more feasible because no objective lens is necessary [5]. Most importantly, full information about both amplitude and phase of the transmitted electric field is recovered. In this paper we describe how nonlinear interactions, which preserve the coherence of the sources used to generate them, can also be used for PCDI. We demonstrate nonlinear PCDI based on second harmonic generation, which is used to image the reversal of the sign of the nonlinear coefficients in a periodically-poled lithium niobate (PPLN) crystal and crystals of 4-nitro-4' methylbenzylidene aniline (NMBA). However, nonlinear PCDI is applicable to all nonlinear microscopy techniques, and the ability to recover phase and amplitude of the generated light can significantly extend the capability of nonlinear imaging.

2. Method

The CDI experimental setup used here is relatively simple, requiring only a coherent source, in this case a femtosecond Ti:sapphire laser, which irradiates an object. The scattered light intensity from the object is collected by microscope lenses that optimally magnify the far field diffraction pattern and image it on a CCD detector (as shown in

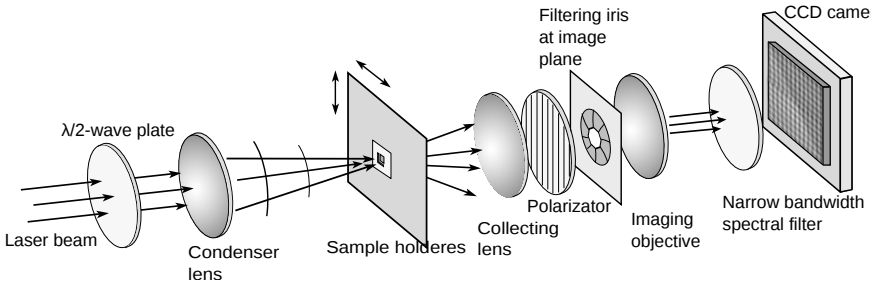

Fig. 1. A simplified schema of the SHG CDI setup. A high intensity beam with linear polarization is focused on the sample. Scattered light is collected by a lens (NA=0.4) and the required polarization is selected. An iris placed at an image plane created by the collecting lens provides a virtual aperture to limit the illuminated region, known as the 'probe'. The transmitted light is imaged through a narrow bandwidth filter onto a CCD. placed out of the imaging plane.

Fig. 1). In this paper, we use a scanning CDI algorithm known as ptychography [6, 7], which is particularly effective and robust at reconstructing phase.

In a linear ptychography experiment, the coherent probe beam which illuminates the sample is scanned over many overlapping regions of a sample, and a scattered intensity pattern recorded at each probe position. The spatial overlap of the adjacent illuminated regions provides one of the constraints necessary for algorithmic phase retrieval; the second is that the scattered intensity matches the measured values. For each illumination position, the electric field just after the sample, the exit wave field, $E(\mathbf{r})$, can be represented as the product of an object transmission function, $O(\mathbf{r})$, and a probe field $P(\mathbf{r}-\mathbf{R_n})$, where the vectors $\mathbf{R_n}$ represent the relative shift of probe beam in the sample coordinate system when recording the n^{th} diffraction pattern, $E(\mathbf{r}) = P(\mathbf{r}-\mathbf{R_n})O(\mathbf{r})$. The ptychography algorithm allows these two components to be separately determined, providing information about the electric field of the probe and the complex transmission function of the object.

The recovered information in a nonlinear ptychography experiment is conceptually different from that obtained from linear ptychography. In the case of nonlinear ptychography, no illumination probe at the imaging wavelength exists. The generated light at the second harmonic of the laser is produced only by the probe beam's nonlinear interaction with the sample. To illustrate what is measured in a nonlinear ptychography experiment, we consider the case of second harmonic generation in a transparent medium. For a second order nonlinearity, the generated electric field polarised along coordinate axis j, E_{3j} , propagating along a transparent nonlinear crystal of length l may be written as [8]:

$$E_{3j} = -\mathrm{i}\omega 2\sqrt{\frac{\mu_0}{\varepsilon}} d'_{jik} E_{1i} E_{2k} \frac{\exp(\mathrm{i}\Delta k l) - 1}{\mathrm{i}\Delta k} \tag{1}$$

where ω is the source frequency, d'_{ijk} is the appropriate nonlinear coefficient, Δk is the phase mismatch[1], and $E_{1i,k}$ and E_{3j} are the input and exit fields along the x, z, and y

[1] If the sample is also absorptive, then the Δk term includes the effect of linear absorption.

axis respectively. In an SHG experiment, field $E_1 = E_2$, and $i = k$, and field E_3 is at 2ω. In a nonlinear ptychography measurement, the exit wave at the second harmonic can be written as the product of those components which track the movement of the probe, and those that are fixed in the sample frame. The integrated exit wave field after the sample, in the simple case of no depletion of the input field, can be written as:

$$E_{3j}(\mathbf{r}) = -2\mathrm{i}\omega\sqrt{\mu_0}E_{1i}(\mathbf{r}-\mathbf{R}_n)^2\left[\sqrt{\frac{1}{\varepsilon(\mathbf{r})}}\frac{\exp[\mathrm{i}\Delta k(\mathbf{r})l(\mathbf{r})]-1}{\mathrm{i}\Delta k(\mathbf{r})}d'_{jik}(\mathbf{r})\right] \qquad (2)$$

where the dependence of each quantity on either probe or object coordinates has been shown explicitly. Thus the nonlinear ptychography process separately recovers one term that depends on the square (not the square modulus) of the input electric field, and a second that depends on the product of the dielectric constant, nonlinear coefficient, and the phasematching factor at any particular position in the object. The ability to measure the complex values of these two factors separately is important in that it provides a significant amount of extra information compared to both linear ptychography and traditional nonlinear microscopy. For example, any variation in the phase of d_{ijk} is observable directly in the square bracketed term of Eq. 2, referred to here as the *nonlinear conversion factor*.

3. Results

To demonstrate the effectiveness of the nonlinear ptychography technique, SHG images of two samples are measured in this work. The first sample is a periodically poled lithium niobate (PPLN) crystal on a glass substrate, provided by Covesion Ltd. PPLN is a nonlinear optical crystal manufactured with a periodic reversal in the sign of the nonlinear coefficient; the well-controlled nature of the poling process in PPLN allows for a detailed knowledge of the crystal orientation, making this an ideal demonstration of the nonlinear CDI technique. The second sample is a polycrystalline sample of 4-nitro-4'-methylbenzylidene aniline (NMBA), an organic nonlinear material.

The experimental arrangement is shown in Fig 1. Samples were illuminated by a Coherent MIRA femtosecond Ti:sapphire laser, with an output power of 460 mW at a wavelength of 800 nm and 120 fs pulse length. The laser beam was focused onto the sample using a 25 cm focal length lens, resulting in FWHM spot size of 90 μm and a Rayleigh range of over 8 mm. The resulting peak intensity on the sample was $2.8{\cdot}10^5$ W/mm^2. The sample was positioned in focus of the beam in order to achieve close to flat illumination wavefront and thus avoid anizotropy of the sample effecting the ptychography overlap constrain. The scattered light was collected by a 0.4 NA microscope objective and imaged onto an iris. A weak diffuser was placed in the imaging plane in order to create a sharp virtual illumination probe with random variation of phase, to improve the reconstruction quality [9]. Imaging of either the fundamental wavelength or the second harmonic could be performed by changing a narrow-bandwidth filter in the beam path just before the detector. After filtering, the scattered light was imaged on to a 16-bit CCD camera (PIXIS 1024B) placed near to the Fourier plane. The dynamic range of the camera was extended by collecting multiple frames with different exposure times. Readout and dark noise were measured and subtracted

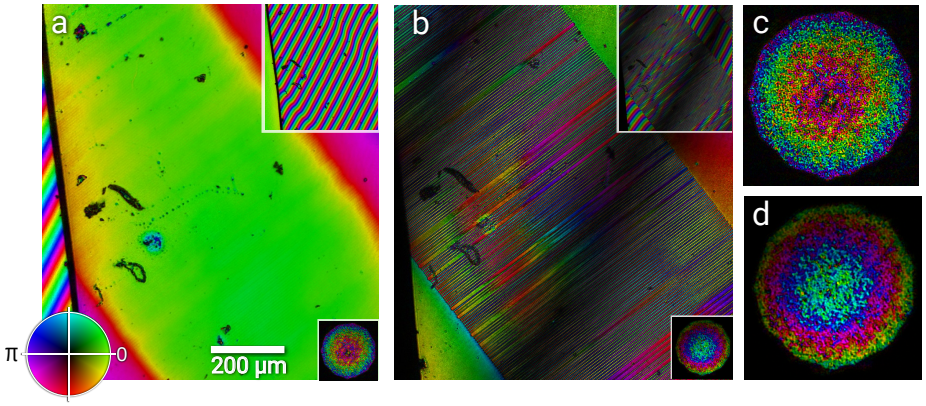

Fig. 2. (a) shows the reconstructed complex linear transmission of the PPLN sample at 400 nm, with a phase ramp due to the sample thickness variation subtracted to show small variation in transmission phase. The upper inset shows the data including the phase ramp, and provides an accurate value of the thickness variation of the wedged sample. The lower inset shows the virtual illumination probe to scale. 2(b) shows the reconstructed nonlinear conversion factor, with significant variation due to the changes in phasematching and d_{ijk} across the sample. Again, the upper inset shows the reconstructed data before phase ramp subtraction. The lower inset shows the virtual probe to scale, as before. 2(c) and 2(d) show magnified images of the virtual illumination probe in the linear experiment (c) and the SHG experiment (d).

from the acquired images. In order to limit the acquisition time, only the central region of 512×512 pixels was collected. The maximum exposure time for the PPLN SHG experiments was 5 s per scanning position, and in total 1185 diffraction patterns were collected to create the image in Fig. 2. The step size of the spiral scan was 30 μm, with 150 μm probe diameter, resulting in an 80% linear overlap between the illuminated regions. Linear oversampling of the diffraction pattern was approximately 3. The resolution is diffraction-limited at 0.5 μm. The reconstruction was performed by the ePIE algorithm [10].

Figure 2 shows reconstructed images of the PPLN sample using (a) linear ptychography using a 400 nm radiation source, and (b) nonlinear ptychography, illuminating at 800 nm and collecting the second harmonic of the illuminating radiation at 400 nm. In (a), the quantity imaged in the linear ptychography measurement is the optical transmission of the PPLN sample at 400 nm. The lower right inset is the recovered virtual illumination probe, to scale. The upper right inset shows the transmission including the phase variation produced by the wedged sample. When the phase ramp is removed (main image), a small variation of the optical thickness can be seen between the broad periodically-poled stripe and the unpoled area.

Figure 2(b) shows the same sample area, but in this case the image is obtained from nonlinear ptychography, with 800 nm light incident on the PPLN sample, and 400 nm light collected at the detector. Again, the lower right inset is the recovered virtual illumination probe, to scale. In this case the image intensity represents the nonlinear

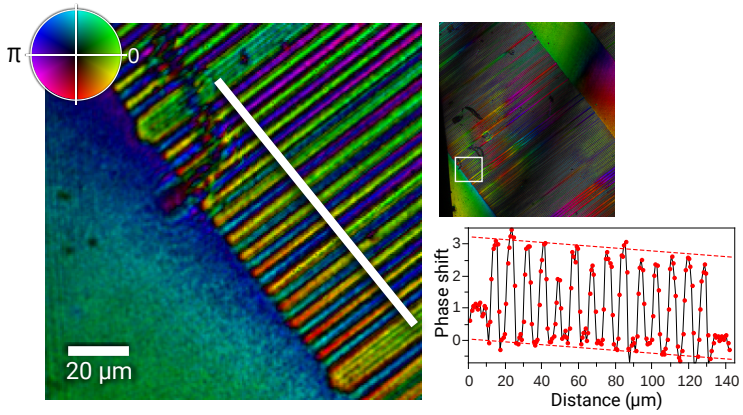

Fig. 3. Close-up of poled region. The left hand image is a close-up of the region shown in the white square in the upper right hand image. The lower right hand image shows a cross-section along the white line of the phase of the nonlinear conversion factor. The dotted lines are spaced by π, and the phase jumps can be seen to have a value of π in areas where the poling is regular

conversion factor described above, the product of the refractive index, the nonlinear coefficient, and the phasematching term. Phase shifts can be seen between the poled and unpoled regions of the grating. Additionally, dark stripes can be seen running from top right to bottom left of the image. Figure 2(c) shows the complex electric field of the illumination probe, obtained from the linear ptychography measurement. Figure 2(d) shows the virtual probe proportional to the square of the complex electric field driving the SHG. In both cases the fields passed through a diffuser and an iris before they are incident on the detector, producing the observed complex structure on the probes.

The phase shift between adjacent poled regions of the lithium niobate is shown at higher magnification in figure 3. The right-hand top image shows the position of the magnified region within the SHG image (white box). In the left-hand, magnified region, the phase change between the poled and unpoled regions of the PPLN grating are clearly visible for most of the poled periods. Where poling has been unsuccessful, the phase shift is missing. A small phase shift between the unpoled regions of the grating and the surrounding unpoled material is also visible. The lower right hand figure shows a cross-section of the phase profile along the white line. The π phase shifts are clearly visible in this cross-section. The measured period of the PPLN grating obtained from this cross-section is 6.99 μm, which compares well with the designed period of 6.94 μm. There is also a small drift in the overall phase, which is associated with the sample thickness variation.

The π phase shift in the effective nonlinear transmission measured from poled and unpoled regions of the PPLN grating arises from the d_{ijk} term in Eq. 2. In lithium niobate, the crystal symmetry dictates that only three independent coefficients exist for the second order nonlinearity [11]. SHG due to propagation along the z axis accesses the d_{22} coefficient. Reversal of the direction of the crystal z axis reverses the sign of the nonlinear coefficient, and hence reverses the phase of the second harmonic gener-

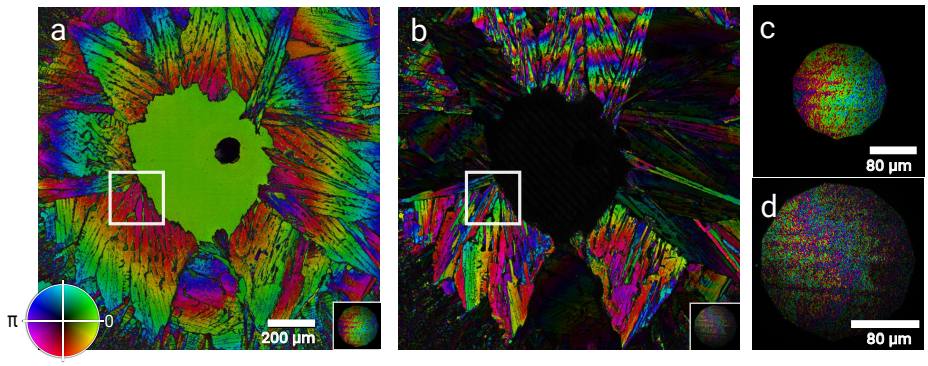

Fig. 4. Images of the (a) linear transmission and (b) nonlinear conversion factor for a polycrystalline sample of NMBA. The insets show the virtual illumination probe, to scale. (c) and (d) show enlarged versions of the virtual illumination probe structure.

ated by the sample. As the recovered image from nonlinear ptychographic imaging is directly proportional to d_{ijk}, its sign is also reversed.

Variation of the amplitude of the nonlinear conversion factor is seen in the dark bars running from bottom left to top right of the right-hand top image shown in figure 3. Because the sample is wedged, the phasematching element of the nonlinear conversion factor varies smoothly across the sample. At any position where the sample thickness is a multiple of twice the coherence length for SHG (given by $\frac{\pi}{\Delta k}$), the amplitude of the second harmonic signal will be reduced to zero. The lateral separation of the two dark bars observable in figure 3 is 597 nm. The change in sample thickness over this distance can be measured from the phase variation seen in the linear optical transmission, shown in the upper right inset to figure 2(b). From this phase variation the sample thickness gradient was measured to be 3.78 nm/μm. From the Sellmeyer equation for MgO-doped PPLN [12], the coherence length for propagation along the z axis can be calculated to be 1.125 μm. Thus the separation of the two dark bars should be equivalent to a sample thickness change of twice the coherence length, or 2.25 μm. The measured thickness change equivalent to twice the coherence length is 2.255 μm, in very good agreement with the calculated coherence length. Similar experiments using shorter duration (40 fs) laser pulses showed no similar dark bars, because the broader frequency width of the pulses results in a distribution of coherence lengths, averaging out the modulation in agreement with calculations. We note that in this test sample, the observed SHG only arises from the last $\approx 2\,\mu$m of the sample.

Figure 4 shows nonlinear ptychography of a more complex sample, in this case a polycrystalline sample of the organic nonlinear material 4-nitro-4'methylbenzylidene aniline (NMBA). NMBA is monoclinic and tends to crystallize in platelets with the crystallographic b axis normal to the platelet [13]. NMBA is highly birefringent and strongly attenuating at 400 nm, and the coherence lengths for SHG when propagating along the b axis are approximately 0.4 μm and 10 μm for the two principal dielectric axes, much closer to the thickness of the sample itself than in the case of PPLN.

Figure 4(a) is a linear ptychographic image taken using linearly-polarised light at

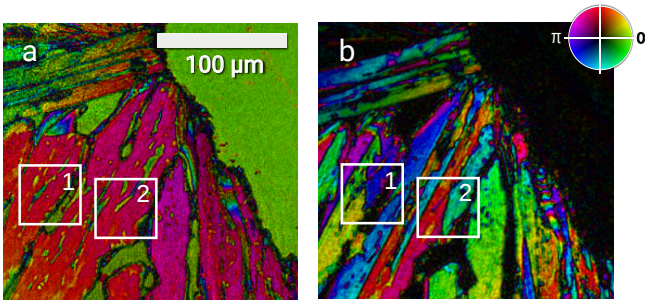

Fig. 5. (a) Linear transmission and (b) nonlinear conversion factor. The boxed regions show areas where the linear transmission shows little variation, but the phase of the nonlinear conversion factor is changed by π, indicating a reversal of the sign of the nonlinear coefficient due to a reversal of the crystallographic b-axis).

800 nm; 4(b) is the nonlinear SHG ptychographic image of the same sample, taken using linear-polarised 800 nm pulsed excitation and recorded at 400 nm. The phase variation indicated by the colour variation in the linear image (a) is caused by anisotropy of the refractive index of NMBA for different crystal platelet orientations, and small changes in sample thickness. The central unvarying region is where the NMBA has been removed, and only the glass substrate is left.

4. Conclusion

The nonlinear ptychographic image shows clearly that for some crystallites, the nonlinear conversion factor is very low, and no signal is observed. This effect is strongly polarization dependent. The complexity of the crystallite structure makes it difficult to assign these changes to a particular component of the nonlinear conversion factor. However, in a number of positions within the crystal, sharp changes in phase can be seen in the SHG image that have no corresponding feature in the linear image. Figure 5 shows the magnified linear (a) and SHG (b) images of the region indicated by the white square in Fig. 4. The boxes labelled 1 and 2 in each picture indicate regions of the sample where no strong spatial variation of the phase or amplitude of the linear transmission can be seen in a particular crystallite in image (a), but a π phase change can be seen in the spatial variation of the SHG image (b). This π phase change can only be due to a change of one of the components of the nonlinear conversion factor that is independent of refractive index and sample thickness; the most likely explanation is that the crystal axes in this area are inverted due to twinning, producing a change of sign of the nonlinear coefficient similar to that seen in PPLN. This change in the crystal structure would be invisible in a normal SHG microscope, and in a linear transmission measurement, even with a measurement of the optical phase. It would also be very hard to detect in an X-ray crystallographic measurement.

In summary, we have demonstrated a generalization of the process of coherent diffractive imaging into the area of nonlinear optics by performing ptychographic imaging of the second harmonic generated from different samples. We have shown that the information available from a nonlinear ptychography experiment is much richer than

either a linear ptychography experiment or a traditional SHG microscopy experiment, in that phase and amplitude information can be obtained separately about both the driving fields and also the nonlinear conversion factor, which represents the product of refractive index, nonlinearity, and phasematching effects. This allows imaging of processes like reversal of crystal axes, which would be invisible in a traditional nonlinear microscopy experiment. Nonlinear CDI has the potential to be applied to many areas of nonlinear microscopy, such as third harmonic generation imaging or CARS microscopy, where the extra information will be valuable in interpreting the image.

Acknowledgements

This work builds on the investment and research from the EPSRC Basic Technology grant GR/R87307/01. M.O. acknowledges financial support from the EU FP7 Erasmus Mundus Joint Doctorate Programme EXTATIC under framework partnership agreement FPA-2012-0033 and and P.B. acknowledges the EPSRC studentship. The K5200 graphics card used for this research was donated by the NVIDIA Corporation. The laser used in this work was provided by the EPSRC Laser Loan Pool. We thank Paul Gow and Tina Parsonage for development of earlier versions of the experimental apparatus, and Matt Parsons for assistance in sample preparation. The data for this work is accessible through the University of Southampton Institutional Research Repository (DOI: 10.5258/SOTON/386425).